

A Micro Strain Gauge with Mechanical Amplifier

Liwei Lin, Albert P. Pisano, and Roger T. Howe, *Fellow, IEEE*

Abstract—A passive micro strain gauge with a mechanical amplifier has been designed, analyzed, and tested. The mechanical amplifier provides a high gain such that residual strain in thin films can be directly measured under an optical microscope. This strain gauge can be *in situ* fabricated with active micro sensors or actuators for monitoring residual strain effects, and both tensile and compressive residual strains can be measured via the strain gauge. It is shown that a very fine resolution of 0.001% strain readouts can be achieved for a micro strain gauge with a 500- μm -long indicator beam. Beam theories have been used to analyze the strain gauge with a mechanical amplifier, and the results were verified by a finite-element analysis. Experimental measurements of both polysilicon and silicon-riched silicon-nitride thin films fabricated by surface micromachining processes are presented. [259]

Index Terms—Mechanical amplifier, residual strain, stress, thin films.

NOMENCLATURE

C	Correction factor.
F	Force.
L	Length of a beam.
M	Moment.
d	Ratio of the width of the indicator beam over the length of the slope beam.
h	Thickness of a beam.
k	Stiffness of a beam.
r	Radius of a beam with semicircular shape.
w	Width of a beam.
ε	Strain.
δ	Movement.
θ	Angular deflection.

Subscripts

v	Vernier gauge.
ib	Indicator beam.
sb	Slope beam.
tb	Test beam.
sc	Semicircular shape.
com	Compressive.

Manuscript received March 4, 1997; revised June 24, 1997. Subject Editor, W. Benecke. This work was supported in part by the Berkeley Sensor and Actuator Center, an NSF/Industry/University Cooperative Research Center, where the devices were fabricated in the UC Berkeley Microfabrication Laboratory, and the finite-element simulation was supported by the Industrial Technology and Research Institute (ITRI), Taiwan.

L. Lin is with the Department of Mechanical Engineering and Applied Mechanics, University of Michigan, Ann Arbor, MI 48109-2125 USA.

A. P. Pisano is with the Department of Mechanical Engineering, University of California at Berkeley, Berkeley, CA 94720 USA.

R. T. Howe is with the Department of Electrical Engineering and Computer Science, University of California at Berkeley, Berkeley, CA 94720 USA.

Publisher Item Identifier S 1057-7157(97)08454-0.

I. INTRODUCTION

A KNOWLEDGE of the mechanical properties of thin films as deposited is important for microelectromechanical systems (MEMS) researchers. Residual strain existing in the thin films is one of the most common properties to be characterized since it affects the device performances. Unacceptably high residual strains may even cause buckling, warpage, or other damages. A good measurement device is essential to monitor and characterize residual strains during microfabrications. Previously, Guckel *et al.* have utilized a proof structure method by using the beam-buckling method for characterizing compressive residual strain [1] as well as used ring structures for determining tensile residual strain [2]. However, since an entire array of structures was needed in the implementation, these previously described structures are not so easily integrated with active micro structures due to space constraints. As opposed to proof structures, one may use Vernier gauges to optically measure the displacement of structures due to the residual strains, and this idea has been used by Kim *et al.* for direct measurement of residual strains [3]. They used a device consisted of two Cantilever beams, fixed at two opposite points. The end movement of the beams caused by the residual strain was measured by a Vernier gauge. This method requires only one structure, but the best resolution for strain measurement reported was only 0.02% for 500- μm beams. One drawback for the Vernier gauge device is that an erroneous strain readout may result if an out-of-plane strain gradient occurs [4].

Many other kinds of strain measurement devices have been proposed. One kind is comprised of T- and H-shape structures [5], [6], which measure the movement at top of the T- or H-shape structure due to residual strain after the structure has been released. Another kind is a strain-magnification structure, which determines strain by interconnecting two opposed beams such that the residual strain in the beams causes a third beam to rotate as a gauge needle. The rotation of the gauge needle quantifies the residual strain. One of these strain gauges requires very long beams (greater than 2.5 mm) [7] to obtain optically readable outputs. The others have strain-gauge designs with shorter beams in the range of tens to hundreds of micrometers, and very fine resolutions can be achieved [8], [9]. Recently, a bent-beam structure has also been developed for strain measurements [10]. Overall, these structures are “complicated” such that very often their behavior cannot be readily determined analytically.

In addition to the above methods (which utilize a specific microstructure fabricated on the wafer specifically for strain measurement purposes), other methods of determining residual

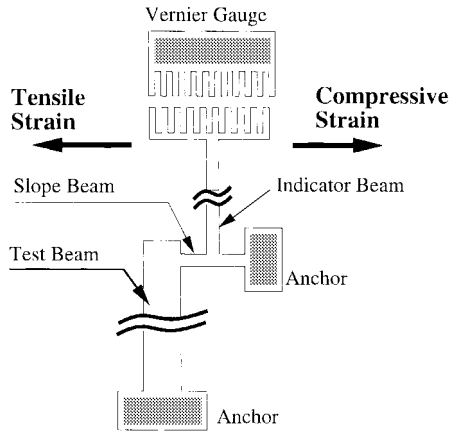


Fig. 1. Schematic diagram of a strain gauge based on the mechanical amplifier.

strains or stresses have been developed, but these require extra equipment and effort. These methods measure special values of thin films and computationally extract residual stresses from these values. For example, the deflections of pressurized thin-film membranes can be measured by microscope [5], probe [11], or laser [12]; the deflections of stressed beams can be measured by probe [11], scanning electron microscope (SEM) [13]; the frequency response of microstructures can be measured by laser [14], spectrum analyzer [15]; and the curvature of the whole wafer can be measured by a flat gage. All these methods require special equipment, and the residual stresses are extracted from the above measured data, which strongly depend on the dimensions (width and thickness) of the thin-film structures, and the uncertainties of these dimensions are the main sources of inaccuracy in addition to the instrumental error.

This paper presents a mechanical micro strain gauge which uses only one structure, can be fabricated *in situ* with active devices, determines tensile or compressive strain under optical microscopes, and has a fine resolution of 0.001%. Moreover, simple beam theory is sufficient for analyzing the measured displacement to determine the *in-situ* residual strain. The accuracy of this strain gauge is greatly improved because its output is independent of both the thickness of the deposited thin film and the cross section of the micro structure. Thus, this new device is insensitive to the dimensional variations that may introduce systematic errors in other methods.

II. STRAIN-GAUGE DESIGN AND FABRICATION

The schematic diagram of the strain gauge is shown in Fig. 1. It consists of three beams, a test beam, a slope beam, and an indicator beam for different purposes. The idea is to mechanically amplify the tiny displacement caused by the residual strain between the two fixed anchors, one at the end of the test beam and the other at the end of the slope beam. Residual strain existing in the thin film causes the test beam to either elongate (compressive residual strain) or shrink (tensile residual strain). Since the test beam is fixed at the anchor end, the other end of the test beam should either elongate or shrink. The same movement will be transferred to the slope

TABLE I
TYPICAL DESIGN VALUES OF THE MICRO STRAIN GAUGE

Symbol	Element	Value
L_{tb}	length of the test beam	500 μm
L_{sb}	length of the slope beam	20 μm
L_{ib}	length of the indicator beam	500 μm
w_{tb}	width of the test beam	30 μm
w_{sb}	width of the slope beam	1.2 μm
w_{ib}	width of the indicator beam	2 μm
h	thickness of thin film	2 μm
w_v	width of the vernier finger	1 μm
L_v	length of the vernier finger	4 μm
	center-to-center distance of vernier fingers	3 μm
	gap between top and bottom vernier fingers	2 μm

beam. This tiny movement at the test beam side of the slope beam creates a maximum, but tiny rotation at the center of the slope beam since the other end of the slope beam is a fixed anchor. The indicator beam, which is placed at the center of the slope beam, magnifies this tiny rotation, and a large displacement (which can be observed under an optical microscope) is generated at the site of the Vernier gauge. Either tensile or compressive strain can be identified immediately after the microfabrication process by inspecting the device under an optical microscope.

The configuration of this micro strain gauge could be incorporated in most of the microfabrication processes. Only two masks are needed for the strain-gauge fabrication, an anchor mask and a structure mask. The SEM photo in Fig. 2 shows two fabricated strain gauges with different lengths of indicator beams. The one on the left-hand side has an indicator beam of 500 μm in length and the one on the right-hand side has of 250 μm . Table I lists their dimensions in detail. The enlarged view of the slope beam which is suspended above the substrate is shown in Fig. 3. The strain gauge is ready for reading after it is released from the substrate by etching away a sacrificial layer.

The micro photo of Fig. 4 demonstrated an example of strain reading under an optical microscope. The position of the Vernier gauge is shown after the release etch. The bottom scale was originally in line with the top two scale markers of the top Vernier gauge. It can be easily observed that the scale has moved to the left, which means a tensile strain occurred. The notches on the top Vernier gauge have a separation of 3 μm , and the tip was best matched at the number eighth tip of the top scale, which results in 1.6 μm of movement at the Vernier gauge. The residual strain is then calculated.

III. MODELING

A. Beam Analysis

One of the advantages of this strain-gauge design is that the structure is simple and a strength of materials beam analysis could result an accurate model. A view of the slope beam is shown in Fig. 5, in which one may observe the fixed-fixed boundary conditions of the ends of the test beams and a small displacement δ_{tb} due to a tensile residual stress. This

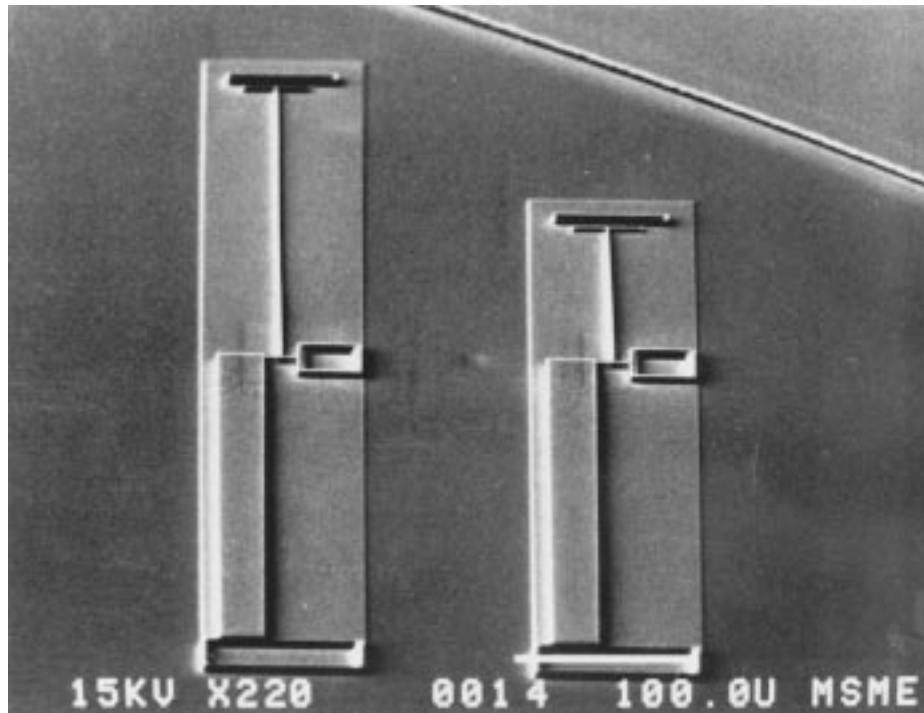


Fig. 2. SEM microphoto of two strain gauges.

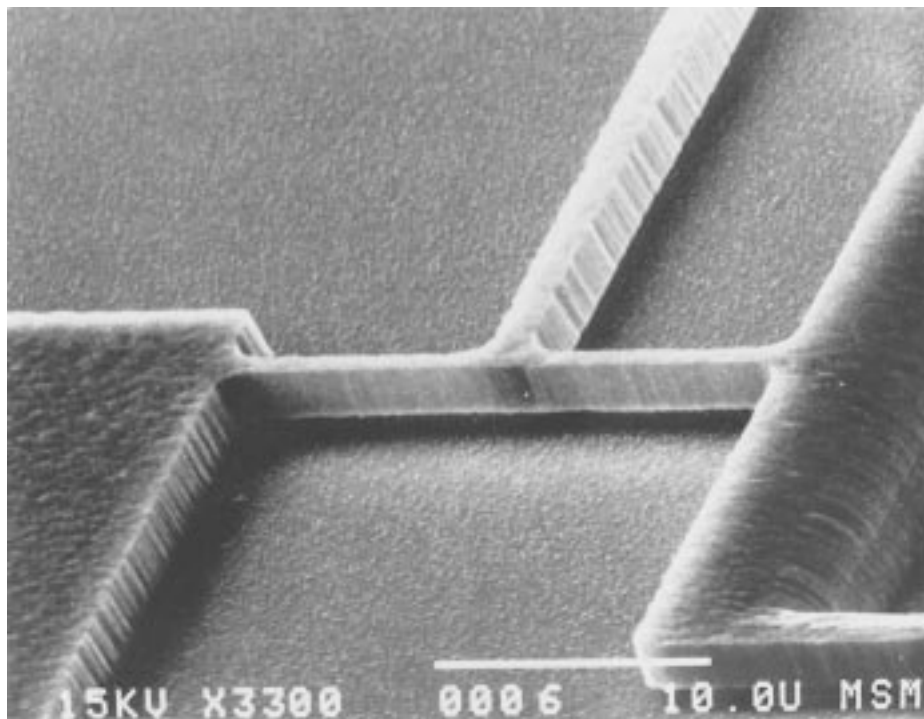


Fig. 3. A close-view SEM photo showing the slope beam.

displacement, which has been exaggerated in the figure, creates tiny angular deflections along the slope beam. F_{tb} and F_{sb} are forces produced by residual stress in the test and slope beam, respectively. M_{tb} ($= F_{tb}L_{sb}$) is the resistant moment due the residual stress in the test beam and is much larger than M_{sb} ($= F_{sb}\delta_{tb}$), the resistant moment due to the residual stress in the slope beam. M_{sb} is neglected and is not drawn in the

figure. The displacement caused by the residual stress in the slope beam is negligible and is also neglected. The maximum angle occurs at the center of the slope beam, where it locates the indicator beam.

Beam analysis can be carried out such that the deflected shape of the slope beam can be derived [16]. The angle of deflection at the center of the slope beam can be represented

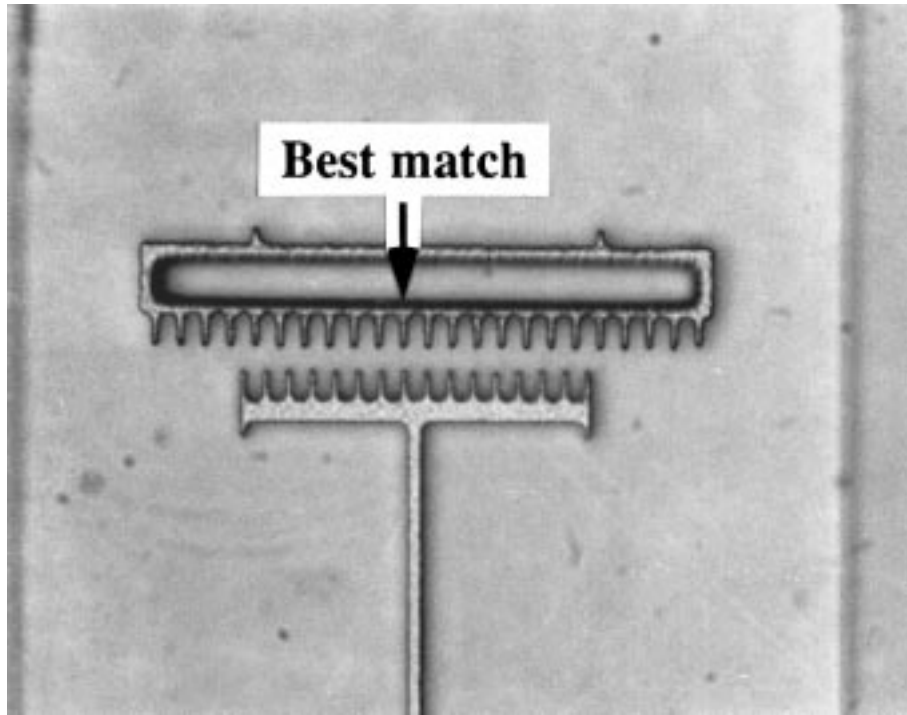


Fig. 4. An example of strain-gauge reading under an optical microscope.

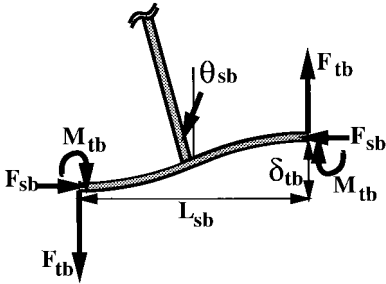


Fig. 5. The force and moment free body diagram of the slope beam.

as

$$\theta_{sb} \approx \tan(\theta_{sb}) = \frac{3\delta_{tb}C}{2L_{sb}} \quad (1)$$

where δ_{tb} is the movement of the test beam caused by the residual strain and L_{sb} is the length of the slope beam. It is noted that (1) is only valid for small θ_{sb} . C is a correction factor due to the presence of the indicator beam and is derived as

$$C = \frac{1-d^2}{1-d^3} \quad (2)$$

where d is the ratio of the width of the indicator beam w_{ib} over the length of the slope beam L_{sb} . The value is very close to one and can be neglected since L_{sb} is much larger than w_{ib} . For the designed strain-gauge dimensions listed in Table I, the value of C is 0.997.

This mechanism provide an mechanical amplification such that the tiny movement of δ_{tb} is magnified to a value of δ_v and the mechanical gain is

$$\frac{\delta_v}{\delta_{tb}} = \frac{3L_{ib}C}{2L_{sb}} \quad (3)$$

where δ_v is the measured movement at the Vernier gauge site. For the designed strain-gauge dimensions listed in Table I, the mechanical amplifier has a gain of 37.4. The residual strain is the ratio of δ_{tb} over the length of the test beam L_{tb} and can be represented as

$$\varepsilon = \frac{2L_{sb}\delta_v}{3L_{ib}L_{tb}C} \quad (4)$$

The significance of the above equation is that this strain gauge gives a strain reading which is independent of the thin-film thickness, a key factor of error for other methods. Moreover, this reading is independent of process variations, which may result irregular beam cross section, for example, a trapezoidal shape [17]. Therefore, this kind of process imperfection is not a problem for the strain-gauge measurement presented here.

B. Model Verification and Limitations

Several effects are considered here for both the optimal designs and implicit limitations of the strain gauge.

1) *Residual Stress in the Slope Beam*: First, the residual stress in the slope beam is considered. As shown in Fig. 5, the unreleased residual stress in the slope beam generate an opposite moment, $M_{sb} = F_{sb}\delta_{tb}$, where M_{sb} and F_{sb} are the moment and force generated by the residual stress in the slope beam. This term has not been considered in the previous assumptions. Nevertheless, it can shown that this effect is negligible compared with the moment M_{tb} generated by the residual stress in the test beam

$$\frac{M_{sb}}{M_{tb}} = \frac{\varepsilon w_{tb}^3 L_{sb}^3}{4L_{tb}^3 w_{sb}^3} \ll 1 \quad (5)$$

where M_{sb} and M_{tb} are moments generated due to the residual stress in the slope beam and the test beam, respectively. Since L_{tb} is designed to be much larger than L_{sb} and ε has a small value, the above assumption is valid.

2) *Stiffness of the Slope Beam*: Second, the stiffness of the slope beam $k_{sb,tb}$ in the direction of displacement due to the residual strain in the test beam should be relatively small such that it does not affect the displacement of the test beam

$$\frac{k_{sb,tb}}{k_{tb,tb}} = \frac{L_{tb}w_{sb}^3}{L_{sb}^3w_{tb}} \ll 1 \quad (6)$$

where $k_{sb,tb}$ is the stiffness of the slope beam in the test beam direction and $k_{tb,tb}$ is the stiffness of the test beam in the test beam direction. For typical design dimensions (listed in Table I), a value of 0.0036 is derived, which is small.

3) *Buckling Effect in the Test Beam*: The buckling effect could occur when a large compressive strain along the test beam even though the slope beam is relatively soft. The following equation shows this effect:

$$\varepsilon_{\max, \text{com}} \leq \frac{\pi^2 h^2 w_{tb} L_{sb}^3}{3 w_{sb}^3 L_{tb}^3} \quad (7)$$

where $\varepsilon_{\max, \text{com}}$ is the maximum compressive strain could be encountered by the strain gauge before causing buckling of the test beam. For the design values list in Table I, this maximum compressive strain can be measured by the current micro strain-gauge design is 1.46%, which is large enough for most cases.

4) *Buckling Effect in the Slope Beam*: In addition to the buckling effect on the test beam, the slope beam may be susceptible to buckling as well. The buckling criterion is derived below

$$\varepsilon_{\max, \text{com}} \leq \frac{4\pi^2 h^2 w_{sb} L_{tb}^2}{3 L_{sb}^2 w_{tb}^3}, \quad \text{if } w_{sb} > h \quad (8)$$

$$\varepsilon_{\max, \text{com}} \leq \frac{4\pi^2 w_{sb}^3 L_{tb}^2}{3 L_{sb}^2 w_{tb}^3}, \quad \text{if } w_{sb} < h. \quad (9)$$

For the standard designed dimensions, the maximum value of the strain is 52.6% and is large. In the case of measuring very large compressive strain, it is suggested to changing the strain-gauge design dimensions according to (7)–(9) to avoid the buckling of the beams.

C. Error Analysis and Finite-Element Simulation

1) *Error Analysis*: A first-order error analysis can be carried out by examining (4), where δ_v , the reading of the Vernier gauge, is the main source of error while other dimensions have negligible error effects. The resolution of δ_v is mainly determined by the design of the Vernier gauge. With the design parameters listed in Table I, a best resolution of 0.2 μm and uncertainty of 0.1 μm can be achieved as shown in Fig. 4. The sharp tips observed in Fig. 4 are the result of overetching in the patterning step. This effect actually helps identifying the correct reading of the Vernier gauge movements. The strain reading with error bound can be represented as

$$\varepsilon = \frac{2L_{sb}\delta_v}{3L_{tb}L_{tb}C} \left(1 \pm \frac{0.1}{\delta_v} \right) \quad (10)$$

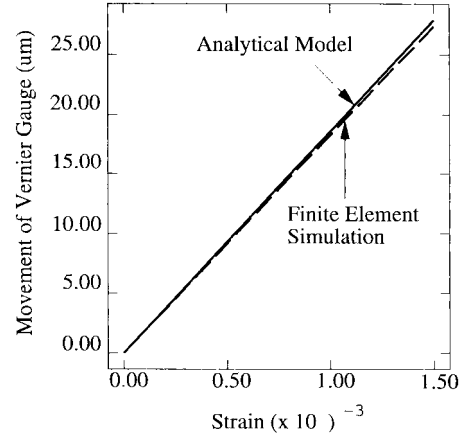


Fig. 6. Theoretical and finite-element simulation results of the movement of Vernier gauge under different strains.

and the best resolution of the strain reading for the designed strain gauge listed in Table I is 0.001%.

As discussed before, the backward force generated by the slope beam and the negative moment effect generated by the residual stresses in the slope beam have been neglected. These effects result in a negligible underestimation of the strain-gauge readings.

2) *Finite-Element Analysis*: Finite-element analysis has been implemented by a software package, ANSYS [18], to check the analytical theories. Strain was introduced by applying a uniform temperature change to the strain-gauge structure with a specified thermal expansion coefficient. Fig. 6 shows the results of movement at the site of Vernier gage versus strain from both the analytical model and a finite-element analysis. The simulation only goes to a residual strain value of 0.0015, which corresponds to a large displacement of more than 25 μm at the site of Vernier gauge. It is found that the theoretical model matches well with finite-element simulations results and there is no nonlinear effects within this region. For the same Vernier movement, the theoretical model underestimates the real strain. A maximum discrepancy of only 1.7% occurs when there is a high strain value of 0.0015, which is negligible in most of the engineering applications. This difference comes mostly from the resistance of the slope beam, which has been neglected in the theoretical model.

IV. EXPERIMENTAL RESULTS AND DISCUSSIONS

These strain gauges have been fabricated via the polysilicon surface micromachining process previously used for lateral resonators [19], with a polysilicon thickness of approximately 2 μm . The annealing process of 950 $^{\circ}\text{C}$ for 2 h was first tested, and a residual tensile strain of 0.017% was observed. Other wafers were then put into another 1000 $^{\circ}\text{C}$ annealing for 2 h, and the residual strain reduced to about 0%–0.001% compressive.

The low-pressure chemical vapor deposition (LPCVD) silicon-rich silicon-nitride films have also been tested by a two-mask process. The phosphorus-doped glass (PSG) is deposited on silicon substrate for the sacrificial layer and

TABLE II
TEST RESULTS OF RESIDUAL STRAINS IN DIFFERENT THIN FILMS

Test	Material	Deposition	Anneal	Strain
(a)	LPCVD polysilicon	605°C, 550mTorr SiH ₄ = 250sccm	950°C, 2 hours	0.017% Tensile
(b)	LPCVD polysilicon	605°C, 550mTorr SiH ₄ = 250sccm	950°C, 2 hours 1000°C, 2 hours	0.001% Compressive
(c)	LPCVD nitride	835°C, DCS = 64sccm 300mTorr, NH ₃ = 16sccm	No	0.032% Tensile

anchors were defined by the anchor mask. A layer of 1.5 μm of LPCVD nitride is deposited at 835 °C with SiCl₂H₂ : NH₃ flow rate of 4:1. The strain gauge is then defined with the second mask and etched in a plasma etcher. The PSG layer is removed in 5:1 buffered hydrofluoric acid (HF) to release the strain gauges. A value of 0.032% tensile strain is observed, and a tensile residual stress of 96 MPa is resulted if 300 GPa is used for the Young's modulus of the silicon-riched nitride. This residual stress is near the reported value, 105 MPa, tensile, by other researchers [20]. All these results are detailed in Table II.

With this micro residual strain gauge, a *local* knowledge of residual strain distribution is possible. The entire polysilicon wafer described in Table II (case A) has been studied, and it has been determined that the residual strain varies over the surface of the wafer. Fig. 7 shows the histogram of the Vernier gauge measurements for 54 different dice (1 cm \times 1 cm in size) averaged distributed on the same 4-in wafer. The coefficient of variation (COV) is approximately 10%, and strain at the edges of the wafer has larger deviations than the center. Theoretically, these variations may come from the slightly irregular random side shapes of the micro beams as seen in Fig. 3. Grain sizes and orientation of the thin-film material may also affect the readings. A probabilistic analysis [21], which used a random grain and geometric uncertainty model, has been performed to calculate effects from the above variations. It has been predicted that 1.14% (COV) comes from the random grain distribution when the grain size is about 1 μm . Another 1.56% coefficient of variation is resulted if the beam-width variation is 6%. The above statistical analysis predicts less than 3% total COV, which does not compare with the experimental result of 10% COV as seen in Fig. 7. The theory only provides explanation of the variation in strain readings based on measuring *identical* strains. In reality, the strain distribution throughout one wafer may differ. Further investigations in the area of micro-scale material behavior are necessary to explain this phenomenon, and the strain gauge described in this paper is a perfect tool to conduct this study.

In addition to the two-mask process described above, a one-mask process has also been demonstrated for characterizing residual strain of thin films. This one-mask process can be implemented by increasing the area of anchors such that these strain gauges can survive the time etching of the sacrificial layer. The SEM photo of a strain gauge made by this one-mask process is shown in Fig. 8. It also shows a symmetrical design in Fig. 8, where a second slope beam has been put on

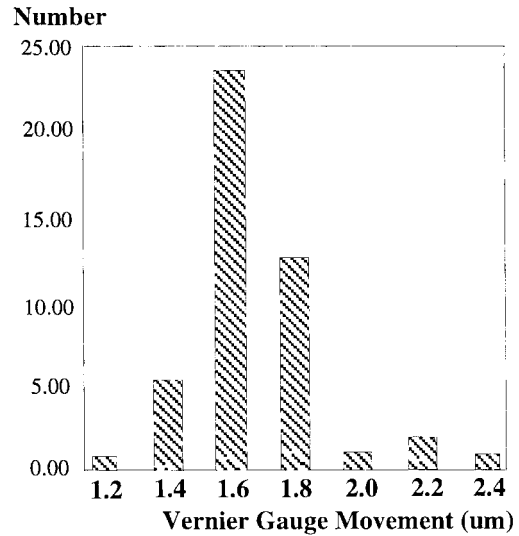


Fig. 7. Histogram of the strain readings on 54 dies of a 4-in wafer.

the opposite site of the test beam with another anchor. This symmetrical design and the one-sided design give same strain readouts, but the symmetrical design is easier to buckle since residual stress in the slope beams cannot be released. This could be demonstrated by the following criterion:

$$\varepsilon_{\max, \text{com}} \leq \frac{\pi^2 h^2}{3L_{\text{sb}}^2}, \quad \text{if } w_{\text{sb}} > h \quad (11)$$

$$\varepsilon_{\max, \text{com}} \leq \frac{\pi^2 w_{\text{sb}}^2}{3L_{\text{sb}}^2}, \quad \text{if } w_{\text{sb}} < h. \quad (12)$$

For the designed dimensions listed in Table I, the maximum value of $\varepsilon_{\max, \text{com}}$ is 1.18%. Hence, the design dimensions need to be modified for larger compressive residual strain measurements.

In addition to the process variations, different types of strain gages may be designed based on similar mechanical magnification schemes. For example, slope beams in the shape of a semicircle as shown in Fig. 9 have been designed and tested together with the straight beams design presented in this paper. The strain readout of a slope beam with semicircular shape is predicted by the elastic theory

$$\varepsilon = \frac{\pi r_{\text{sb}} \delta_v}{2L_{\text{ib}} L_{\text{tb}} C_{\text{sc}}} \quad (13)$$

where δ_v is the measured displacement at the Vernier site, r_{sb} is the radius of the slope beam with semicircular shape, and C_{sc} is the correction factor due to the presence of the

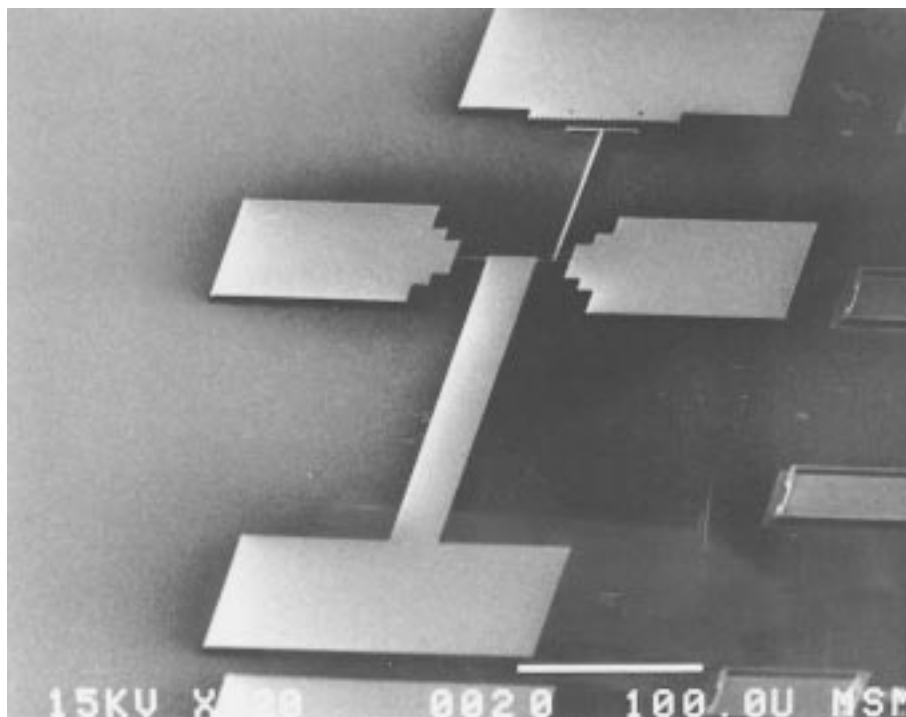


Fig. 8. SEM microphoto of a strain gauge fabricated by a one-mask process.

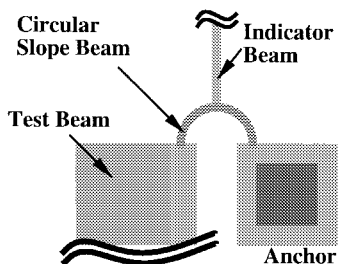


Fig. 9. Schematic diagram of the a slope beam with semicircular shape.

indicator beam at the center of the circular slope beam. It can be represented as

$$C_{sc} = \frac{\cos(d)}{1 - \frac{2}{\pi} \left[d_{sc} - \frac{\sin(2d_{sc})}{2} \right]} \quad (14)$$

where d has the same definition as before and d_{sc} is the ratio of the width of the indicator beam w_{ib} over the radius of the slope beam r_{sb} . The value of C_{sc} is very close to one and can be neglected in most cases. Theoretically, the readings of the slope beams with semicircular shape should be slightly less than those of straight shape slope beams with the same nominal dimensions. This difference has been observed experimentally. In addition, strain-gauge designs with slope beams in the shape of crab legs [22] and with curved Vernier scales [23] (to make possible the reading of yet larger strains) have all been proposed. Nevertheless, the current strain-gauge design with straight shape slope beams has the advantages of higher magnification factor and simpler mechanical analysis.

The thickness of the thin film will not cause the reading errors, but it is advised of having a thicker layer for the testing purpose. An LPCVD silicon-nitride film with just

0.1 μm of thickness has been tried and, the reading can be obtained only if the releasing of the strain gauge was carefully performed. These extra thin-film structures tend to break or become distorted out of plane. Apparently, they have little vertical and lateral resistance to the disturbance of rinsing liquids, which produce relatively large surface-tension forces during the drying process. However, for structures thicker than 0.45 μm , these phenomena seldom happen. Another design suggestion is to make the sacrificial layer thicker. It is found that a 0.1- μm -thick sacrificial layer may cause a severe sticking problem and drastically reduce the yield of readouts.

Sticking has been one of the major problems for surface micro structures, but it has little effect on the strain gauge. The slope beams at the end of the test beam provide enough strength which not only prevents the test beam from sticking, but also provides a resistant force that prevents the test beam from curling if an out-of-plane strain gradient exists. In case that sticking becomes a severe problem, it is advised to leave a shallow layer of deionized (DI) water on the wafer while observing the reading. Occasionally, a small amount of sticking is actually a benefit. When an out-of-plane strain gradient exists, it is easier to observe the reading under microscope if the indicator beam sticks slightly to the substrate. However, in presence of high negative strain gradients, the movable part of the Vernier gauge bend upwards, and it is difficult to focus the microscope to both parts of the gauge simultaneously. An artificial marker can be used to replace the fixed part of the Vernier gauge on a TV screen to solve this problem. This marker can be made of paper by focusing, drawing, and taping the shape of the fixed part of the Vernier gauge on the TV screen. The movement of the

Vernier gauge can be obtained by focusing the microscope to the movable part of the Vernier gauge and using the artificial marker on the TV screen as the reference. The bent-beam strain-gauge design as demonstrated by Gianchandani and Najafi [10] can circumvent this problem without using the artificial marker.

V. CONCLUSIONS

A passive micro strain gauge based on the mechanical amplification technique has been designed, demonstrated, and characterized. This strain gauge can be fabricated *in situ* along with active micro sensors or actuators on the same chip for monitoring residual strain effects. Both tensile or compressive strain could be easily observed under optical microscopes, and with the help of a Vernier gauge design, the resolution of strains as small as 0.001% could be achieved. A simple strength of material analysis based on the theory of elastic beams has been used to model the strain-gauge behavior. This model has been verified by a finite-element analysis. It is found that the theoretical analysis only underestimates the residual strain value of 1.7% less than the real value when the residual strain reaches a high value of 0.15%. These residual strain gauges have been successfully used in surface micromachining processes to measure thin-film residual strains for both polysilicon and silicon-nitride thin films.

ACKNOWLEDGMENT

The authors would like to thank P. Krulevitch and G. Fedder for valuable discussions.

REFERENCES

- [1] H. Guckel, T. Randazzo, and D. W. Burns, "A simple technique for the determination of mechanical strain in thin films with applications to polysilicon," *J. Appl. Phys.*, vol. 57, pp. 1671-1675, 1985.
- [2] H. Guckel, D. W. Burns, C. C. G. Visser, H. A. C. Tilmans, and D. Deroo, "Fine-grained polysilicon films with built-in tensile strain," *IEEE Trans. Electron Devices*, vol. 35, pp. 800-801, June 1988.
- [3] C. J. Kim, "Silicon electromechanical microgrippers: Design, fabrication, and testing," Ph.D. dissertation, M.E. Dept., Univ. California, Berkeley, 1991.
- [4] L.-S. Fan, R. S. Muller, W. Yun, R. T. Howe, and J. Huang, "Spiral microstructures for the measurement of average strain gradients in thin films," in *Proc. IEEE Workshop Microelectromechanical Syst., MEMS'90*, pp. 177-181.
- [5] M. G. Allen, M. Mehregany, R. T. Howe, and S. D. Senturia, "Microfabricated structures for the *in situ* measurement of residual stress, Young's modulus, and ultimate strain of thin films," *Appl. Phys. Lett.*, vol. 51, pp. 241-243, 1987.
- [6] M. Mehregany, R. T. Howe, and S. D. Senturia, "Novel microstructures for the *in situ* measurement of mechanical properties of thin films," *J. of Appl. Phys.*, vol. 62, pp. 3579-3584, 1987.
- [7] L. B. Wilner, "Strain and strain relief in highly doped silicon," in *Dig. IEEE Solid-State Sensor Actuator Workshop*, 1992, pp. 76-77.
- [8] J. F. L. Goosen, B. P. van Driehhuizen, P. J. French, and R. F. Wolfenbittel, "Stress measurement structures for micromachined sensors," in *Dig. Transducers'93, Int. Conf. Solid-State Sensors and Actuators*, 1993, pp. 783-786.
- [9] F. Ericson, S. Greek, J. Söderkvist, and J.-A. Schweitz, "High sensitive internal film stress measurement by an improved micromachined indicator structure," in *Dig. Transducers'95, Int. Conf. Solid-State Sensors and Actuators*, 1995, vol. 2, pp. 84-87.
- [10] Y. B. Gianchandani and K. Najafi, "Bent-beam strain sensors," *IEEE J. Microelectromech. Syst.*, vol. 5, pp. 52-58, 1996.
- [11] R. J. Jaccodine and W. A. Schlegel, "Measurements of strains at Si-SiO₂ interface," *J. Appl. Phys.*, vol. 37, pp. 2429-2434, May 1966.
- [12] E. I. Bromley, J. N. Randall, D. C. Flanders, and R. W. Mountain, "A technique for the determination of stress in thin films," *J. Vac. Sci. Technol. B*, vol. 1, pp. 1364-1366, 1983.
- [13] R. T. Howe and R. S. Muller, "Stress in polycrystalline and amorphous silicon thin films," *J. Appl. Phys.*, vol. 54, pp. 4674-4675, 1983.
- [14] L. M. Zhang, D. Uttamchandani, and B. Culshaw, "Measurement of the mechanical properties of silicon microresonators," *Sens. Actuators A-Phys.*, vol. 29, pp. 79-84, Sept. 1991.
- [15] R. I. Pratt, G. C. Johnson, R. T. Howe, and J. C. Chang, "Micromechanical structures for thin film characterization," in *Dig. Transducers'91, Int. Conf. Solid-State Sensors and Actuators*, 1991, pp. 205-208.
- [16] H. Dubbel, *Handbook of Mechanical Engineering*. New York: Springer-Verlag, 1994.
- [17] W. C. Tang, M. G. Lim, and R. T. Howe, "Electrostatic comb drive levitation and control method," *J. Microelectromechanical Syst.*, vol. 1, pp. 170-178, 1992.
- [18] ANSYS, *Finite Element Analysis Program*, ANSYS, Inc., Canonsburg, PA, 1996.
- [19] W. C. Tang, T. C. Nguyen, and R. T. Howe, "Laterally driven polysilicon resonant microstructures," *Sens. Actuators*, vol. 20, pp. 25-32, 1989.
- [20] R. A. Stewart, J. Kim, E. S. Kim, R. M. White, and R. S. Muller, "Young's modulus and residual stress of LPCVD silicon-rich silicon nitride determined from membrane deflection," *Sensors and Materials*, vol. 2, pp. 285-297, 1991.
- [21] D. Mirfendereski, L. Lin, A. D. Kiureghian, and A. P. Pisano, "Probabilistic response of micro-fabricated polysilicon beam structures: Comparison of analysis and experiments," in *Proc. ASME Winter Annu. Meet., Symp. Micromechanical Syst.*, Nov. 1993, vol. DSC-46, pp. 77-80.
- [22] G. K. Fedder, "Simulation of microelectromechanical systems," Ph.D. dissertation, EECS Dept., Univ. California, Berkeley, 1994.
- [23] P. Krulevitch, M.E. Dept., Univ. California, Berkeley, personal communication.



Liwei Lin received the B.S. degree in power mechanical engineering from National Tsing Hua University, Taiwan, R.O.C., in 1986, and the M.S. and Ph.D. degrees in mechanical engineering from the University of California, Berkeley, in 1991 and 1993, respectively.

He was with BEI Electronics Inc. from 1993 to 1994, in the research and development of micro-sensors. From 1994 to 1996, he was an Associate Professor in the Institute of Applied Mechanics, National Taiwan University, Taiwan. Since 1996, he has been an Assistant Professor at the Mechanical Engineering and Applied Mechanics Department at the University of Michigan. He joined the Berkeley Sensor & Actuator Center, an NSF/Industry/University research cooperative center as a research assistant during his graduate study. His research interests include microelectromechanical systems, including design, modeling, and fabrication of microstructures, microsensors, and microactuators. He has four U.S. patents in the area of MEMS.



Albert P. Pisano received the Ph.D. degree in high-speed camshaft systems from Columbia University, New York, in 1981.

He is currently the DARPA/ETO MEMS Program Manager, and is on administrative leave from his permanent position as Full Professor in the Department of Mechanical Engineering at the University of California, Berkeley. He is jointly appointed in the Department of Electrical Engineering and Computer Science and serves as a Codirector on the Berkeley Sensor and Actuator Center, and NSF/Industry/University Cooperative Research Center. He has been a Member of Research Staff in the Mechanical Engineering Sciences Area of the Xerox Palo Alto Research Center. He has also held research positions at the General Motors Research Laboratory. In MEMS, he has been active in the design, optimization, and fabrication of resonant structure micromotors, micromechanical grippers, and micro test apparatus for friction and impact measurements.

Dr. Pisano was honored in 1985 with the NSF Presidential Young Investigation Award for research in optimal mechanical systems design.



Roger T. Howe (S'79–M'84–SM'94–F'96) was born in Sacramento, CA, on April 2, 1957. He received the B.S. degree in physics from Harvey Mudd College, Claremont, CA, in 1979, and the M.S. and Ph.D. degrees in electrical engineering from the University of California at Berkeley in 1981 and 1984, respectively.

He was on the faculty of Carnegie-Mellon University, Pittsburgh, PA, during the 1984–1985 academic year, and was an Assistant Professor at the Massachusetts Institute of Technology, Cambridge, from 1985 to 1987. In 1987, he moved to the University of California at Berkeley, where he is now a Professor in the Departments of Electrical Engineering and Computer Sciences and Mechanical Engineering, as well as a Director of the Berkeley Sensor & Actuator Center. His research interests include silicon microsensors and microactuators, micromachining processes, and assembly processes.

Dr. Howe served as Cogeneral Chairman of the 1990 IEEE Micro Electro Mechanical Systems Workshop and was General Chairman of the 1996 Solid-State Sensor and Actuator Workshop, Hilton Head, SC.